Accepted Manuscript

Comparison of different label-free imaging high-throughput biosensing systems for aptamer binding measurements using thrombin aptamers

Christin Rath, Juergen Burger, Leo Norval, Stefan Daniel Kraemer, Nicole Gensch, Alexander van der Kooi, Christine Reinemann, Ciara O'Sullivan, Marketa Svobodova, Guenter Roth

Please cite this article as: C. Rath, J. Burger, L. Norval, S.D. Kraemer, N. Gensch, A. van der Kooi, C. Reinemann, C. O'Sullivan, M. Svobodova, G. Roth, Comparison of different label-free imaging high-throughput biosensing systems for aptamer binding measurements using thrombin aptamers, *Analytical Biochemistry* (2019), doi: https://doi.org/10.1016/j.ab.2019.05.012.

Comparison of different label-free imaging high-throughput biosensing systems for aptamer binding measurements using thrombin aptamers

Short title: Label-free imaging biosensing system comparison

Christin Rath[1,2,3,5#], Juergen Burger[1,5], Leo Norval[1], Stefan Daniel Kraemer[1,2], Nicole Gensch[4], Alexander van der Kooi[6], Christine Reinemann[7,8], Ciara O'Sullivan[9,10], Marketa Svobodova[9], Guenter Roth[1,2,3,5]

1 Laboratory for Microarray Copying, Center for Biological Systems Analysis (ZBSA), University of Freiburg, 79104 Freiburg, Germany

2 Faculty for Biology, Biology 3, University of Freiburg, 79104 Freiburg, Germany

3 Centre for Biological Signaling Studies (BIOSS), University of Freiburg, 79104 Freiburg, Germany

4 BIOSS Toolbox, Centre for Biological Signaling Studies (BIOSS), University of Freiburg, 79104 Freiburg, Germany

5 BioCopy GmbH, 79110 Freiburg, Germany

6 IBIS Technologies b.v., 7521 PR Enschede, The Netherlands

7 Helmholtz Centre for Environmental Research GmbH (UFZ), 04318 Leipzig, Germany

8 Present address: Aptamer Group Ltd, Innovation Way, Bio Centre, Heslington, York, YO10 5NY, United Kingdom

9 Departament d'Enginyerı´a Quı´mica, Universitat Rovira i Virgili, 43007 Tarragona, Spain

10 Institucio´ Catalana de Recerca i Estudis Avanc¸ats, 08010 Barcelona, Spain

Corresponding author: christin.rath@zbsa.uni-freiburg.de, tel.: +49 761 203 97154, fax: +49 761 203- 8456

Postal address: Laboratory for Microarray Copying , ZBSA-Center for Biological Systems Analysis, University of Freiburg, Habsburgerstrasse 49, 79104 Freiburg, Germany

Email addresses:

Christin Rath   christin.rath@zbsa.uni-freiburg.de

Juergen Burger   juergen.burger@zbsa.uni-freiburg.de

Leo Norval   leo.norval@students.uni-freiburg.de

Stefan Daniel Kraemer   stefan.kraemer@zbsa.uni-freiburg.de

Nicole Gensch   nicole.gensch@bioss.uni-freiburg.de

Alexander van der Kooi   alex@ibis-spr.nl

Christine Reinemann   christine.reinemann@aptamergroup.co.uk

Ciara O'Sullivan   ciara.osullivan@urv.cat

Marketa Svobodova   marketa.svobodova@urv.cat

Guenter Roth   guenter.roth@zbsa.uni-freiburg.de

ABSTRACT

To enable the analysis of several hundreds to thousands of interactions in parallel, high-throughput systems were developed. We used established thrombin aptamer assays to compare three such high-throughput imaging systems as well as analysis software and user influence. In addition to our own iRIf-system, we applied bscreen and IBIS-MX96. As non-imaging reference systems we used Octet-RED96, Biacore3000, and Monolith-NT.115. In this study we measured 1378 data points. Our results show that all systems are suitable for analyzing binding kinetics, but the kinetic constants as well as the ranking of the selected aptamers depend significantly on the applied system and user. We provide an insight into the signal generation principles, the systems and the results generated for thrombin aptamers. It should contribute to the awareness that binding constants cannot be determined as easily as other constants. Since many parameters like surface chemistry, biosensor type and buffer composition may change binding behavior, the experimenter should be aware that a system and assay dependent KD is determined. Frequently, certain conditions that are best suited for a given biosensing system cannot be transferred to other systems. Therefore, we strongly recommend using at least two different systems in parallel to achieve meaningful results.

KEYWORDS

1.   Introduction

Biosensing systems for the analysis of ligand-target interactions allow the determination of affinity, detailed information about binding kinetics and are of special interest for signaling, molecular network identification and also for drug targeting in pharmacology. To compare different binders and interactants, e.g. to evaluate an inhibitor for a cellular receptor, the analysis of the ligand-target binding behavior and the determination of its KD values is essential for understanding and later prediction. It may even have influence on the decision whether e.g. a pre-drug compound will be followed up as "hit" or simply gets dropped.

As labeling of the molecular targets may have an unpredictable impact on their binding [1,2] and as fluorophores can be quenched by labeled molecules, label-free detection is a desired upcoming method [3–7]. Still, the immobilization of a ligand on a biosensor surface might itself have a very strong influence on the binding properties of the targets. Such label-free biosensing systems do not require labeling steps of ligands or targets, reducing both preparation time and the costs. There is also no structure variation of the analytes and no steric hindrance to immobilized ligands induced by fluorescent dyes. Label-free biosensing allows direct measurement and real-time monitoring of binding events. For this reason, several label-free methods have been developed in recent decades. The most prominent is Surface Plasmon Resonance (SPR) introduced in 1983 by Liedberg et al. [8], which became widespread by Biacore in 1990, and many others followed. Soon afterwards, imaging methods such as SPR imaging (SPRi) [9] were developed and commercialized to open the opportunity of high-throughput screening of hundreds of compounds in parallel in a microarray format.

Rich et al. [10] benchmarked label-free low throughput systems in the early 2000s. We are now taking the first step in the comparison of label-free high-throughput imaging systems. We looked not only at well-known parameters (ligand, target structure, biosensor type, surface chemistry and buffer composition) that influence the kinetics constants, but also at the chosen system, analysis software and user.

In addition to SPR, other methods like ellipsometry [11], reflectometry [12] and interferometry [13] were used for label-free detection on biosensor surfaces. However, such label-free methods can only be applied for high-throughput and highly parallel screening in combination with microarrays and in an imaging manner. Surprisingly, to our knowledge, neither a global calibration standard for such systems nor major comparison studies with such high-throughput systems have been published so far. Existing low-throughput system studies are mainly focused on protein-protein interactions as model system, but are not based on DNA-protein interactions. For our comparison study, we selected well-described thrombin aptamers, which have been partly analyzed by biosensing methods [14–16]. Moreover, we compared the following label-free high-throughput imaging systems and low-throughput non-imaging systems for reference (please note that the listing below was made alphabetically because of its abbreviation and indicates neither a ranking nor a valuing of any system):

- BLI (BioLayer Interferometry) on Octet RED96 (Pall ForteBIO LLC, Fremont, USA)

- iRIf-system [17] (imaging Reflecto-Interferometry), self-made system (Laboratory for microarray copying, University of Freiburg, ZBSA, Freiburg, Germany)

- MST (MicroScale Thermophoresis) on Monolith NT.115 (Nanotemper Technologies GmbH, Munich, Germany)

- SCORE (Single COlour REflectometry) on bscreen (Biametrics GmbH, Tübingen, Germany)

- SPR (Surface Plasmon Resonance) on Biacore3000, (GE Healthcare Lifesciences Corporate, Buckinghamshire, UK)

- SPRi (Imaging Surface Plasmon Resonance) on IBIS MX96 microarray Imager (IBIS Technologies B.V., Enschede, Netherlands)

System details can be found in the supplementary information sections A.1 to A.6.

1.1 The thrombin aptamer assay

As ligands we used the well-characterized thrombin DNA aptamers, which are mainly known as fibrinogen-binding-site and heparin-binding-site aptamers published by Gold and Tuerck and Tasset et al. [18,19]. Aptamers are short, single-stranded DNA or RNA oligonucleotides (typically shorter than 100 nt) able to bind their targets with high affinity, sensitivity and specificity similar to antibodies. Therefore, Aptamers are of great interest as antibody substitutes for research and medical applications (e.g. for analysis, diagnostics, therapeutics, drug discovery and biomarker discovery) because they are easy to synthesize and modify. Jenison et al. [20] found the selectivity of aptamers for some targets to be 10 times better than the selectivity of according antibodies. Depending on the target, the primary aptamer sequence, the sequence length and the buffer composition, aptamers form different three-dimensional shapes like G-quadruplexes, stem loops, bulges, I-motifs, pseudoknots, kissing complexes, triplicates and hairpins [21,22]. The binding of an aptamer to its target is based on a combination of induced-fit mechanism, hydrogen bonds, Van-der-Waals interactions, stacking interactions between aromatic rings and nucleobases as well as electrostatic interactions of charged groups [23].

We chose the two thrombin aptamer consensus sequences (A1 and B1) and also elongated them with T20 spacers (A2 and B2) to analyze the effect of spacer on aptamer target binding. Since it is known that primer sequences from aptamer libraries are often involved in the binding, the full-length aptamers (A3 and B3) were also chosen for comparison. Our primer sequences are compatible to the microarray generation approach described by Hoffmann et al. [24] enabling generation of microarrays with thousands of DNA spots via digital solid-phase PCR. Aptamers against mold proteins [25] were used as negative binding controls (C1 and C2). The specificity of the aptamer thrombin binding was tested beforehand by using a primary anti-thrombin antibody and a secondary FITC-labeled antibody. As a positive target control, Streptavidin-Cy5 was bound to biotinylated BSA. For iRIf and SCORE, we additionally used fluorescent labeled DNA as immobilization efficiency controls.

1.2   System comparison

For our comparison study, we used three label-free high-throughput biosensing systems (iRIf, SCORE and SPRi) and three low-throughput systems (BLI, MST and SPR). Because of the signal generation principle, BLI is comparable to iRIf and SCORE, SPR is the reference for SPRi. MST serves as alternative solution reference for all systems. For maximum comparability, we applied the assay itself as identical as possible. Only the immobilization of the aptamers and the surface chemistry are predefined by the respective system. For the immobilization we also chose a maximum similarity between the systems, if possible (can be found in the supplementary information sections A.1 to A.6). In addition, each biosensing system has its advantages and limitations that are summarized in table 1.

Table 1. Advantages, limitations and costs of each applied method and system (* only 8 aptamers can be measured in one 96-well plate and for each aptamer one biosensor is needed; that means in total 8 biosensors per well plate. # in total 3 channels, because one channel is needed for referencing with aptamer and without thrombin, dp = data points, pub = publication). Total costs for 1000 dp per run/series was also calculated to demonstrate the amortization of microarray format using systems. Label free MST measurements are possible with Monolith NT.LabelFree. **We only considered the systems used in this study**.

[Insert Table 1]

High-throughput systems like iRIf, SCORE and SPRi consume very low material in terms of ligands. They therefore cost the least per data point (dp) and run, unless only a few data points are measured. Consequently, the cost per data point does not decrease linearly with increasing number of data points per run. For 1000 or more data points, the highest cost factor is the analyte and biosensor, not the ligand consumption on the microarray. For BLI and MST, however, the cost generation is exactly the opposite of high-throughput systems, since a new biosensor/capillary and a new analyte sample are required for each data point, so the total costs increases linearly with the number of data points. As SPR requires a reference channel, the costs increase more or less linearly with the number of data points. Therefore, iRIf, SCORE and SPRi are best suited for high-throughput measurements with several hundred or more data points to keep costs as low as possible. For all biosensing systems except MST, the limitation is the required immobilization of one interaction partner, whereas for MST the limitation is the non-measurable kinetics.

2.   Materials and methods

2.1   Materials

Depending on the biosensor type and surface chemistry, the aptamers were modified on their 5' end either with NH2 including a C6 spacer or biotin. With all methods we measured the aptamer sequences shown in table A.7 of the supplementary information (except C1, which was only tested in iRIf and SCORE).

For each biosensing system we immobilized the thrombin aptamers on the respective biosensor surface. The aptamers and control oligonucleotides were ordered from Biomers (Ulm, Germany), human α-Thrombin from Sigma-Aldrich (art. no. T6884, Steinheim, Germany), monoclonal primary anti-thrombin antibody (art. no. ab2087) and polyclonal secondary antibody (art. no. ab7064) from Abcam plc (Cambridge, UK), Bovine serum albumin from CARL ROTH (Karlsruhe, Germany) and Streptavidin-Cy5 from VWR (Darmstadt, Germany). The binding and washing buffer, BB (KC) buffer (pH 7.6), was published by D. Mann et al. [26]. The BB(KC) buffer consists of 20 mM tris-(hydroxymethyl)aminomethane, 100 mM sodium chloride, 2 mM magnesium dichloride, 5 mM potassium chloride, 1 mM calcium dichloride and 0.02 % (v/v) Tween20. As printing and incubation buffer we used 300 mM Sodiumdihydrogenphosphate buffer at pH 8.3 (called NaPi). The Regeneration buffer consists of urea 8.3 M, 340 mM NaCl and 0.05 % (v/v) Tween20. All buffer components were ordered from CARL ROTH (Karlsruhe, Germany). For PDITC chemistry we used (3-aminopropyl)-triethoxysilane (APTES) from ABCR (Karlsruhe, Germany), 1,4-phenylene diisothiocyanate (PDITC) from Sigma-Aldrich (Steinheim, Germany), ethanolamine, isopropanol, acetone, denatured ethanol and double-distilled water from CARL ROTH (Karlsruhe, Germany). For EDC/NHS chemistry and SPR measurements 1-ethyl-3-(3-dimethylaminopropyl)carbodiimide (EDC), N-Hydroxysuccinimid (NHS), Streptavidin, sodium acetate, PBS, ethanolamine, NaCl and NaOH were ordered from Sigma-Aldrich (Barcelona, Spain).

2.2 Surface chemistry methods

The detailed protocols are given in the supplementary information (section A.1 to A.6). The following section will shortly introduce the applied surfaces and chemistries.

BLI (Octet RED96) - Streptavidin coupling: Octet RED96 uses streptavidin coated single-use and disposable biosensors called Dip and Read™ Streptavidin biosensors. The biosensors are hydrated in binding buffer for 10 min before coupling with biotinylated aptamers (Fig. 1A).

iRIf-system (Laboratory for Microarray Copying, Freiburg) - PDITC surface chemistry: A glass slide with a coating of high-refractive thin layers on top is used as biosensor surface. The immobilization of amino-labeled DNA was realized with the PDITC chemistry described by Hoffmann et al. [27] (Fig. 1B). Initially the glass slides are activated for 5 min in an oxygen plasma (Plasma device, Diener electronic (Ebhausen, Germany)) at 100 W. After surface modification the amino-labeled aptamers are spotted and incubated overnight in humid atmosphere.

SCORE (Biametrics GmbH, Tübingen) – NHS surface chemistry: The SCORE biosensor surface of Biametrics is comparable to the iRIf (Fig. 1C), but with different refractive layer compositions. The applied biosensor ("BM-2D array-chip NHS - BMV18207) is activated with active ester chemistry to immobilize amino-labeled DNA.

SPR (Biacore, Laboratory of Ciara O'Sullivan, Tarragona, Spain) – EDC / NHS surface chemistry: A streptavidin modified CM5 chip is used for measurements with a Biacore3000 (Fig. 1D). The surface is activated with EDC/NHS. Afterwards a coating with streptavidin for immobilization of biotinylated aptamers is done.

SPRi (IBIS MX96 Imager) – EDC / NHS surface chemistry: A gold coated biosensor called P-type Streptavidin SensEye is used for SPRi measurements (Fig. 1E). This surface consists of a glass chip with a thin gold and dextran layer. The surface chemistry is quite similar to Biacore3000 (Fig. 1D).

The surface chemistry details can be found at the supplementary information section A.1 to A.6.

[Insert Figure 1 and please print in color; 2-column image]

Figure 1 Schematic overview of surface chemistries used including biosensor surfaces. **(A)** Streptavidin biosensor from Pall FortéBio, **(B)** PDITC chemistry on glass slide with high-refractive layer, **(C)** BM-2D array-chip NHS - BMV18207 biosensor chip from Biametrics providing NHS groups, **(D)** CM5 chip from Biacore activated with EDC / NHS chemistry and streptavidin layer, **(E)** SensEye P Strep sensor from SensEye.

3.   Results

3.1   System comparison

Since each system has a different flow cell and biosensor type, different flow rates, volumes and surface chemistries, we came to the same conclusion as Rich et al [10] – data can be best presented in a scatter plot. The binding curves and kinetics determination were reviewed for each system by an expert from the respective manufacturer to ensure optimal analysis. In total we investigated six different thrombin aptamers, three aptamer modifications of the aptamer that binds to the fibrinogen binding site (A1 to A3) and three of the aptamer that binds to the heparin binding site (B1 to B3). From these reviewed results, we generated the scatter plots (Fig. 2 for aptamer A1 and B1). The scatter plots of aptamer A2, A3, B2 and B3 are shown in the supplementary information section A.17. In total, we generated 1378 data points (all systems included). For retaining an overview, we did not display the error bars in the scatter plots. For our averaged KD value calculation, we only considered statistically relevant data points. As relevant selection criterion for KD average value calculation, we decided to exclude the first 10 % of the highest and the lowest KD values of each data set because of the possibilities of mass transport limitation, surface effects and artifacts. A second criterion was to sort out KD values with standard deviations higher than 50 % of the KD value. All data points that were not considered for KD averaging are displayed in lighter colors in the plots. In addition, we completely removed data points, where fitting was collapsing or not converging. All KD average values including standard deviation are shown in table 2.

Table 2. KD average values and corresponding standard deviations (indicated in nM; are also shown in the supplementary information A.8 with Standard Deviation; except for MST) of all aptamer and thrombin concentrations for each system calculated with the respective analysis software (SW). **#** A3 concentration series measured with BLI. ***** average values of three KD values.

[Insert Table 2]

For KD value determination, we applied the 1:1 kinetic model to each software (for details supplementary information A.9 to A.15). For BLI we used the Octet Data Analysis software 8.2, for iRIf our in-house analysis software Anabel, for MST the MO.Affinity analysis software, for SCORE the b-nd software, for SPR the BIA evaluation software 4.1 and for SPRi the Scrubber2 software. For each system and aptamer at least six thrombin concentrations were measured and analyzed. In accordance to the standard procedures, a typical aptamer concentration was chosen for each system and biosensor type (BLI: 2 µM, iRIf and SCORE: 15 µM, SPR: 2 µM, MST: 20 nM). Except for SPRi, we measured two concentration series (first: 20 nM, 5 nM, 1.25 nM, second: 32 nM, 16 nM, 8 nM, 4 nM, 2 nM, 1 nM) to investigate the influence of surface density on the aptamer binding. A concentration series was also measured exemplarily with BLI for aptamer A3 (Fig. A.17.2 in supplementary information). The SPRi measurements showed no significant differences in the binding constants between the different concentrations. On the other hand, for the BLI measurements, a concentration between 2 µM and 500 nM (KD values: 3.1 to 8.9 nM) seems to be better than a lower concentration of 250 to 125 nM (KD values: 11.3 to 18.9 The KD values (Fig. 2; Fig. A17.1-A17.4 in the supplementary information) for all systems and aptamers except for B2 and B3 are mostly within the nanomolar range. There are even some data points from SPRi measurements determined in the picomolar range. Also for aptamer A1 we measured with MST KD values in the pico- and nanomolar range (2 pM and 52 nM). The lowest KD value is determined with MST (shown as bar) for aptamer A1, which is 2 pM. Whereas the highest value was determined with iRIf for aptamer A1, which is 279 nM. The average KD values (displayed in table 2, **rounded values in scatter plots**) for A1 range from 2 pM to 130 nM (Fig. 2A), A2 from 3 nM to 47 nM (Fig. A.17.1), A3 from 3 nM to 118 nM (Fig. A.17.2), B1 from 2 nM to 86 nM (Fig. 2B), B2 from 1 nM to 85 nM (Fig. A.17.3) and B3 from 1 nM to 60 nM (Fig. A.17.4).

[Insert Figure 2 and please print in color, 2-column image]

Figure 2. (A) Aptamer A1 and **(B)** B1 scatter plot of kass versus kdiss for all systems (filled marks in caption) and kdiss versus kass averages (filled bigger marks with rounded value indication). The number of data points (N) for each system is indicated in the captions. The lighter colored data points were included in the analysis, but were not considered for KD averaging.

.

To visualize the aptamer ranking, the KD average values for each system are presented in a scatter plot (Fig. 3A), except for MST, which are displayed in a bar graph (Fig. 3B). Looking at the plot, it becomes clear that each system has its own KD value range. While most systems measure in the two to three digit range, the SPRi measures KD values in the one digit range. From MST measurements, however, we have obtained KD values from the one- to three-digit range. Furthermore, the ranking of the aptamers differs between the systems. For BLI it was found that aptamer A3 (8 nM and 25.5 nM) is the best binder and A1 (73 nM) the poorest binder, for iRIf aptamer A2 is the best (26.4 nM) and aptamer A1 the poorest (129.8 nM), for MST the B aptamers (B1: 3.4 nM, B2: 5 nM, B3: 7.6 nM) proved to be better binders and as poorest binder aptamer A3 (101.9 nM). For SCORE (Anabel analysis) the best is B1 (9.2 nM) and the poorest A3 (34.6 nM), for SCORE (b-nd analysis) the best are A2 (6.3 nM) and A3 (6.9 nM) and the poorest B1 (37 nM), for SPR A2, B1 and B3 lay in the upper range (17 nM, 15.7 nM, 17.6 nM) and the poorest binder is A3 (117.8 nM). For SPRi all aptamers are within the low nanomolar range from 0.8 to 4.4 nM.

[Insert Figure 3 and please print in color, 2-column image]

Figure 3. Graphical illustration of KD ranking between different aptamers and systems. **(A)** Scatter plot of aptamer KD average values (**rounded values**) for iRlf, SCORE, SPR, BLI and SPRi. **(B)** Bar chart with KD average values (**rounded values**) for MST.

3.2   Analysis software comparison (supplementary information A.18)

To investigate the influence of the analysis software used, we selected five binding curves of aptamer A1 from the BLI data set (272 nM thrombin concentration) and additionally analyzed them with Anabel [28], b-nd software, BIA evaluation software, Scrubber2 software and Origin. As a fitting model, we performed a single curve analysis with identical fitting windows for all software expecting a 1:1 kinetic model. The resulting KD values show an average variance of 0.81 % between the different analysis software with a maximum value of 1.11 % and a minimum value of 0.66 %.

Since each system uses its own software, modeling and analytics including sampling rates and averaging, a 'simple' comparison is not possible. To confirm that the software provides identical results, we generated a generic data transfer file that allows all data to be imported and exchanged with any other analysis software. An exception is the BLI software, since only the export is possible (due to the data encryption no easy import from other systems is possible). As an example, we recalculated and normalized a binding curve of aptamer A3 from each data set and adjusted the sampling rates, averaging and analysis time scales. The on and off kinetic curves between the methods differ from each other (Fig. 4). It may be due to different surfaces, flow rates, mass transport effects and biosensor response times.

[Insert Figure 4 and please print in color, 1.5-column image]

Figure 4. Recalculated and normalized aptamer A3 binding curves for SPRi (purple), BLI (green), SCORE (yellow), iRIf (high time resolution in blue; adapted lower time resolution in dark blue) and SPR (pink).

3.3   User comparison (supplementary information section A.19)

Since selecting the fitting range is critical to the results, we performed a user dependency analysis for KD determination using the Anabel software. We selected a BLI data set with 12 binding curves (Four replicates at three different aptamer A3 concentrations and one thrombin concentration (54 nM)). Eight persons from the laboratory for microarray copying in Freiburg participated in the user comparison. To rule out any influence from knowledge of the data, the binding curves were renamed by an independent person who did not know any results from Figure 2 and A17.1 to A.17.4 at that time. Each participant analyzed all 12 binding curves to the best of their knowledge for kass and kdiss determination. As an example of the binding curve A.1, the highest KD value is 65.6 nM, determined by participant #3, and the lowest 4.5 nM, determined by participant #8, which shows that the values differ by a factor of 14.5 (93.3 %).The smallest variance show the KD values of participant #6 with 16.4 nM and participant #5 with 16.9 nM, which corresponds to a difference of 3 %. And by adding a software error of 1 %, the total user-induced variance would range between 4 % and 94.3 %.

4.   Discussion

4.1   System comparison

Our study showed that the scatter plots for each system have a certain scattering range (up to a factor of 20), as can also be seen in the publication from Rich et al.[10]. This confirms our assumption that various parameters such as biosensor surfaces, surface chemistries and flow cells influence the kinetics and thus the KD determination. Since we also assumed that the binding behavior is strongly influenced by surface effects, which could be indicated by the high KD variance for A1, since this aptamer contains only a small spacer to the surface and could be influenced more strongly than others. Regarding the kinetic model, we observed for each system that the binding does not behave like a 1:1 model, but in some cases more like a 2:1 kinetic model (also published by Hasegawa et al. [29]) with a faster and slower kinetic part (Fig. A.9 to A.15). This indicates that the 1:1 model may not be the appropriate model for the analysis of aptamer thrombin interactions, although it can be found in some literature references [30–32]. In addition, we noticed some possible rearrangement effects, especially in iRIf measurements, that can be observed with a small signal drop after saturation. We believe that the kinetic model may suggest that either two aptamers bind to both thrombin binding sites which should be further proven by competitive measurements, or that thrombin forms a kind of dimer. The binding sites can also be promiscuous, which means that e.g. A1 binds preferably to the fibrinogen binding site, but may also bind to the heparin binding site with a lower KD. This is shown in particular by the fact that we observed two binding events from MST measurements which led to KD values of 52 nM and 2 pM.

4.2   Analysis software comparison

Because of the low KD value variance (from 0.66 % to 1.11 %) between the different analysis software presented in our study, we conclude that comparable results are generated, if exactly the same data set is included in the analysis.

4.3   User comparison

We have shown with our user comparison that the fitting window selected by the user strongly influences the resulting KD values, although the same analysis software is used. We analyzed variances up to a factor of 14.5 when using an identical data set (A.19 in the supplementary information). We come to the conclusion that the fitting depends much more on the respective user than on the software used. The most important factor is the choice of fitting windows, which depends on the experience and skills of users. The KD average values and Standard Deviation for the user comparison are shown in table A.19. Therefore, we strongly recommend that a data set should be analyzed independently by two different users without prior knowledge of the binding assay.

5.   Conclusions

We compared a total of five biosensing systems and found out that the KD values can deviate up to a factor of 20 and that there could be no a real ranking between the observed aptamers due to the variance. From our software comparison we can conclude that the software induces only 1 % difference on the KD value with appropriate operation and setting of the fitting parameters. In fact, the user has much greater influence on the results, which can be up to a factor of 10 in the KD value by analyzing the same data set. Interestingly, Rich et al. [10] also found a variance of factor 10 and more comparing label-free low-throughput non-imaging systems with each other. While Rich et al. focused their comparison only on the systems and not on the influence of software and users, a closer look at their scatter plots shows a similar range to our scatter plots. Rich et al. also reported that some users have fitted their data taking into account transport limitations and drifting baselines, which further increases the variance of KD values. In our study, the same fitting model was used for all data sets, but we still achieved different results. This is clearly due to the choice of fitting windows, which can lead to a change in the KD value of an order of magnitude. Therefore, the skilled user should not only consider that many parameters (applied system, surface chemistry and density, flow cells, assay conditions such as buffers and concentrations) influence the resulting kinetic constants, but also the user is a strong factor influencing the results. Our recommendation is to measure binding interactions with at least two different systems in order to avoid systematic errors such as surface effects and to achieve reliable results. In addition, we recommend that each data set should be analyzed in parallel by two independent, well-trained and skilled users to avoid user biased errors.

Regardless of this, our results show that all systems are suitable for the analysis of binding kinetics and deliver KD values in the nM to pM range. To learn more about the binding behavior of thrombin aptamers, competitive measurements with inhibitors are required. In addition, we will also investigate the binding motif and epitopes by high-throughput measurements of different sequence mutants on microarrays.

Acknowledgements

ORCID iD

Christin Rath   0000-0003-4707-5977

Stefan Daniel Krämer 0000-0002-0071-9344

Günter Roth   0000-0001-9343-6046

Table 1

Method	SPR	BLI	MST	SPRi	iRIf	SCORE
Measurement principle	change of light energy transfer at different angles	interference change at different wavelengths	fluorescence change due to thermophoresis	change of light energy transfer at different angles	interference change of light at one wavelength	interference change of light at one wavelength
Used system	Biacore 3000	Octet RED96	Monolith NT.115	IBIS MX96	iRIf-system	bscreen
Analysis	Label-free & real-time	Label-free & real-time	In solution, by label & real-time	Label-free & real-time imaging	Label-free & real-time imaging	Label-free & real-time imaging
Typically limit of detection (given by manufacturer)	pM-mM	nM-µM	pM-mM	pM-mM	nM-mM	nM-mM
Costs per biosensor [€]	150	10	4	100	80	80
Throughput dp [per run possible]	3[#]	8*	16	96	4 000	22 500
Throughput and consumption in this publication						
Throughput dp / run	3	8	16	48	20	20
≈ Aptamer consumption	400	3 200	6.4	3.2	1.8	1.8

/ run [pmol]						
≈ Thrombin consumption / run [pmol]	28.6	435.2	556	12.8	136	272
≈ Aptamer consumption / dp [pmol]	200	400	0.4	0.07	0.09	0.09
≈ Thrombin consumption / dp [pmol]	9.5	54.4	34.8	12.8	136	272
Costs per data point [€]						
If only 1 dp / run measured	156.41	23.43	4.14	104.7	85	90
In this pub	54.28	23.43	4.14	2.28	4.25	4.50
1000 dp run	54.22	23.43	4.14	1.15	0.09	0.09
Costs per run [€]						
In this pub	162.83	187.43	66.18	109.49	85.05	90.05
1000 dp run	54 222	23 429	4 137	1 154	88	93
Limitations	Immobilization of one interaction partner	Immobilization of one interaction partner	No kinetics measureable	Immobilization of one interaction partner	Immobilization of one interaction partner	Immobilization of one interaction partner

Table 2

| Aptamer	BLI	iRIf	MST	SCORE	SCORE	SPR	SPRi
A1	73 ± 26.8	129.8 ± 74.9	0.0017 ±0.3 51.5 ± 0.6	11.4 ± 4.2	14.8 ± 1.1	98 ± 45.9	4.4 ± 5.3
A2	46.9 ± 16	26.4 ± 15.9	23 ± 0.6	22 ± 5.2	6.3 ± 0.5	17 ± 11	3.3 ± 3.1
A3	25.5 ± 15.4	55.1 ± 24.2	101.9* ± 1.6	34.6 ± 19.9	6.9 ± 0.3	117.8 ± 136.3	2.8 ± 2.6
A3**#**	8 ± 2.9	-	-	-	-	-	-
B1	45.2 ± 19.2	86.4 ± 47.8	3.4 ± 1.5	9.2 ± 7.2	37 ± 3.2	15.7 ± 11.8	2.1 ± 1.6
B2	42 ± 17.4	85.2 ± 41.4	5* ± 1.3	12.1 ± 4.9	17.7 ± 0.8	22.7 ± 13.5	0.8 ± 0.9
B3	33.2 ± 40.2	60.3 ± 38.5	7.6 ± 0.5	26.2 ± 7.7	15.5 ± 0.8	17.6 ± 10	1.4 ± 0.7
C1	-	No binding	-	No binding	No binding	-	-
C2	No binding	No binding	µM range binding	No binding	No binding	No binding	No binding
SW	Octet data anal. SW	Anabel	MO.Affinity anal. SW	Anabel	b-nd	BIA eval. SW	IBIS eval. SW

6. References

[1] B. Salih, R. Zenobi, MALDI Mass Spectrometry of Dye–Peptide and Dye–Protein Complexes, Anal. Chem. 70 (1998) 1536–1543.

[2] L.e.a. Yin, How does fluorescent labeling affect the binding kinetics of proteins with intact cells?, Biosensors & bioelectronics 66 (2015) 412–416.

[3] Seidel, Claus A. M. et al., Nucleobase-Specific Quenching of Fluorescent Dyes. 1. Nucleobase One-Electron Redox Potentials and Their Correlation with Static and Dynamic Quenching Efficiencies, J. Phys. Chem. 100 (1996) 5541–5553.

[4] Nguyen, Dat H. et al., Binding to an RNA Aptamer Changes the Charge Distribution and Conformation of Malachite Green, J. Am. Chem. Soc. 124 (2002) 15081–15084.

[5] Unruh, Jay R. et al., Orientational dynamics and dye-DNA interactions in a dye-labeled DNA aptamer, Biophysical journal 88 (2005) 3455–3465.

[6] A.e.a. Iqbal, Orientation dependence in fluorescent energy transfer between Cy3 and Cy5 terminally attached to double-stranded nucleic acids, Proceedings of the National Academy of Sciences of the United States of America 105 (2008) 11176–11181.

[7] J.e.a. Bao, Label-free solution-based kinetic study of aptamer-small molecule interactions by kinetic capillary electrophoresis with UV detection revealing how kinetics control equilibrium, Anal. Chem. 83 (2011) 8387–8390.

[8] B.e.a. Liedberg, Biosensing with surface plasmon resonance — how it all started, Biosensors and Bioelectronics 10 (1995) i–ix.

[9] Schasfoort R.B.M., Tudos A. J. (Ed.), Handbook of Surface Plasmon Resonance, RSC Publishing, 2008.

[10] R.e.a. Rich, A global benchmark study using affinity-based biosensors, Analytical biochemistry 386 (2009) 194–216.

[11] Davis, R. B. et al., Ellipsometric observations of surface adsorption and molecular interactions of native and modified fibrinogen and factor VIII, Surface Science 96 (1980) 539–554.

[12] P.e.a. Schaaf, Reflectometry as a technique to study the adsorption of human fibrinogen at the silica/solution interface, Langmuir 3 (1987) 1131–1135.

[13] G.e.a. Gauglitz, Chemical and biochemical sensors based on interferometry at thin (multi-) layers, Sensors and Actuators B: Chemical 11 (1993) 21–27.

[14] C.e.a. Polonschii, A novel low-cost and easy to develop functionalization platform. Case study. Aptamer-based detection of thrombin by surface plasmon resonance, Talanta 80 (2010) 2157–2164.

[15] R.e.a. Zichel, Aptamers as a sensitive tool to detect subtle modifications in therapeutic proteins, PloS one 7 (2012) e31948.

[16] G. Mayer (Ed.), Nucleic Acid Aptamers. Selection, Characterization, and Application, Humana Press, New York, NY, 2016.

[17] J.e.a. Burger, Low-Volume Label-Free Detection of Molecule-Protein Interactions on Microarrays by Imaging Reflectometric Interferometry, SLAS technology 22 (2017) 437–446.

[18] C. Tuerk, L. Gold, Systematic evolution of ligands by exponential enrichment. RNA ligands to bacteriophage T4 DNA polymerase, Science (New York, N.Y.) 249 (1990) 505–510.

[19] Tasset, D. M. et al., Oligonucleotide inhibitors of human thrombin that bind distinct epitopes, Journal of molecular biology 272 (1997) 688–698.

[20]   R.e.a. Jenison, High-resolution molecular discrimination by RNA, Science (New York, N.Y.) 263 (1994) 1425–1429.

[21]   D.E. Gilbert, J. Feigon, Multistranded DNA structures, Current Opinion in Structural Biology 9 (1999) 305–314.

[22]   Y. Li, R.R. Breaker, Kinetics of RNA Degradation by Specific Base Catalysis of Transesterification Involving the 2'-Hydroxyl Group, J. Am. Chem. Soc. 121 (1999) 5364–5372.

[23]   T. Hermann, D.J. Patel, Adaptive recognition by nucleic acid aptamers, Science (New York, N.Y.) 287 (2000) 820–825.

[24]   J.e.a. Hoffmann, Solid-phase PCR in a picowell array for immobilizing and arraying 100,000 PCR products to a microscope slide, Lab on a chip 12 (2012) 3049–3054.

[25]   Reinemann C., Aptamere für Biosensoren: Selektion von Aptameren für eine Verwendung als neue molekulare Erkennungselemente in Biosensoren (2009).

[26]   D.e.a. Mann, In vitro selection of DNA aptamers binding ethanolamine, Biochemical and biophysical research communications 338 (2005) 1928–1934.

[27]   J.e.a. Hoffmann, Universal protocol for grafting PCR primers onto various lab-on-a-chip substrates for solid-phase PCR, RSC Adv. 2 (2012) 3885.

[28]   Krämer, Stefan D. et al., Anabel. An Online Tool for the Real-Time Kinetic Analysis of Binding Events, Bioinform Biol Insights 13 (2019) 117793221882138.

[29]   H.e.a. Hasegawa, Improvement of Aptamer Affinity by Dimerization, Sensors (Basel, Switzerland) 8 (2008) 1090–1098.

[30]   Russo Krauss, I. et al., High-resolution structures of two complexes between thrombin and thrombin-binding aptamer shed light on the role of cations in the aptamer inhibitory activity, Nucleic acids research 40 (2012) 8119–8128.

[31]   Russo Krauss, I. et al., Thrombin-aptamer recognition. A revealed ambiguity, Nucleic acids research 39 (2011) 7858–7867.

[32]   Russo Krauss, I. et al., Crystallization and preliminary X-ray analysis of the complex of human alpha-thrombin with a modified thrombin-binding aptamer, Acta crystallographica. Section F, Structural biology and crystallization communications 66 (2010) 961–963.
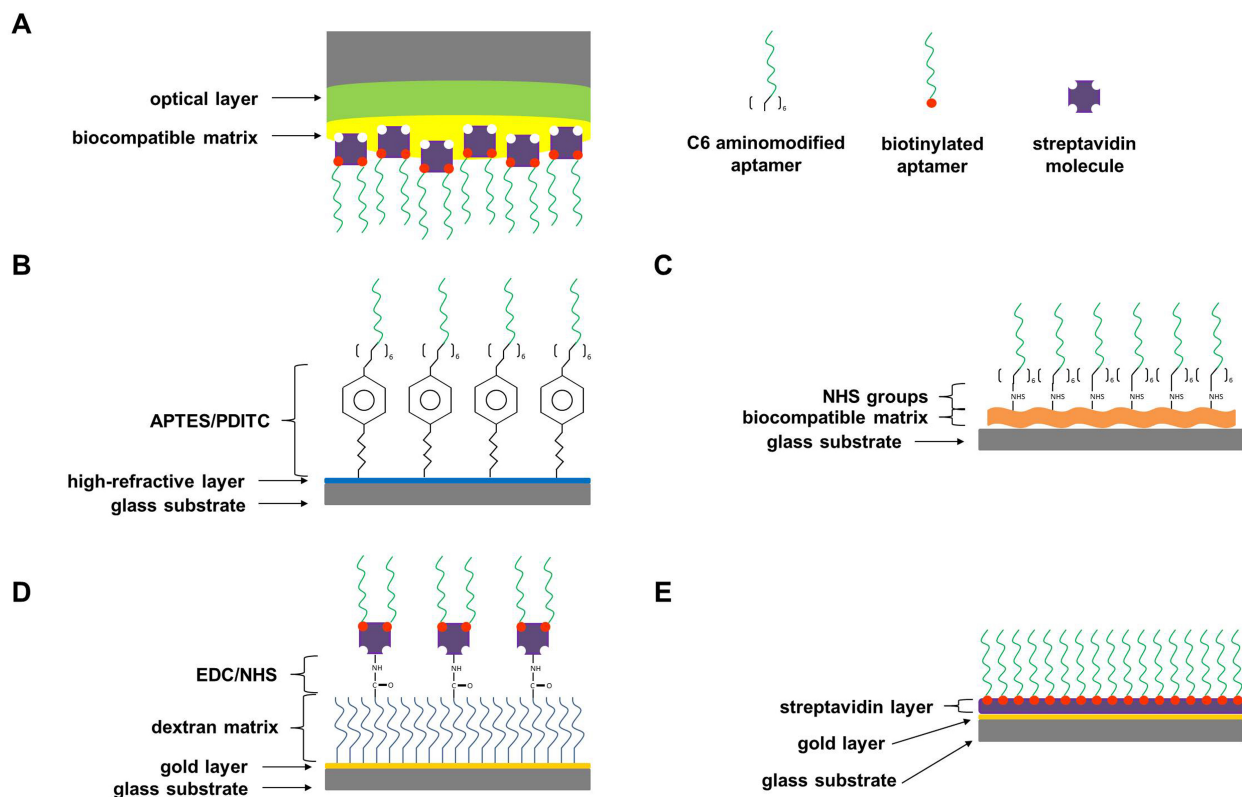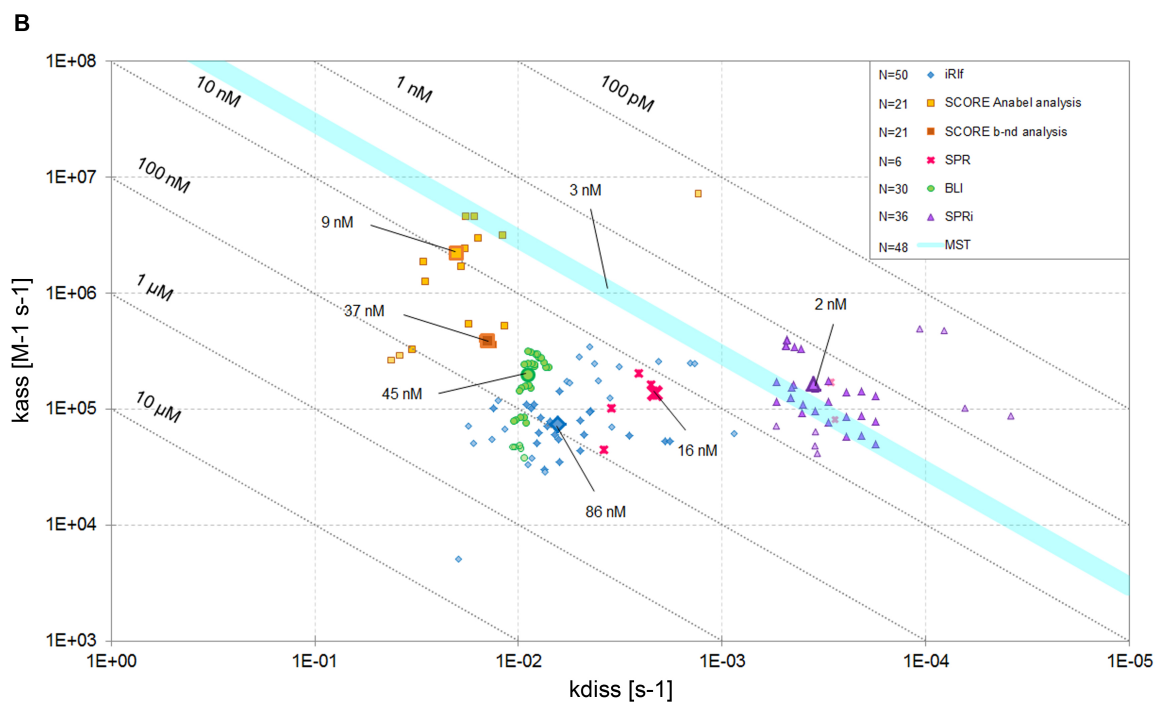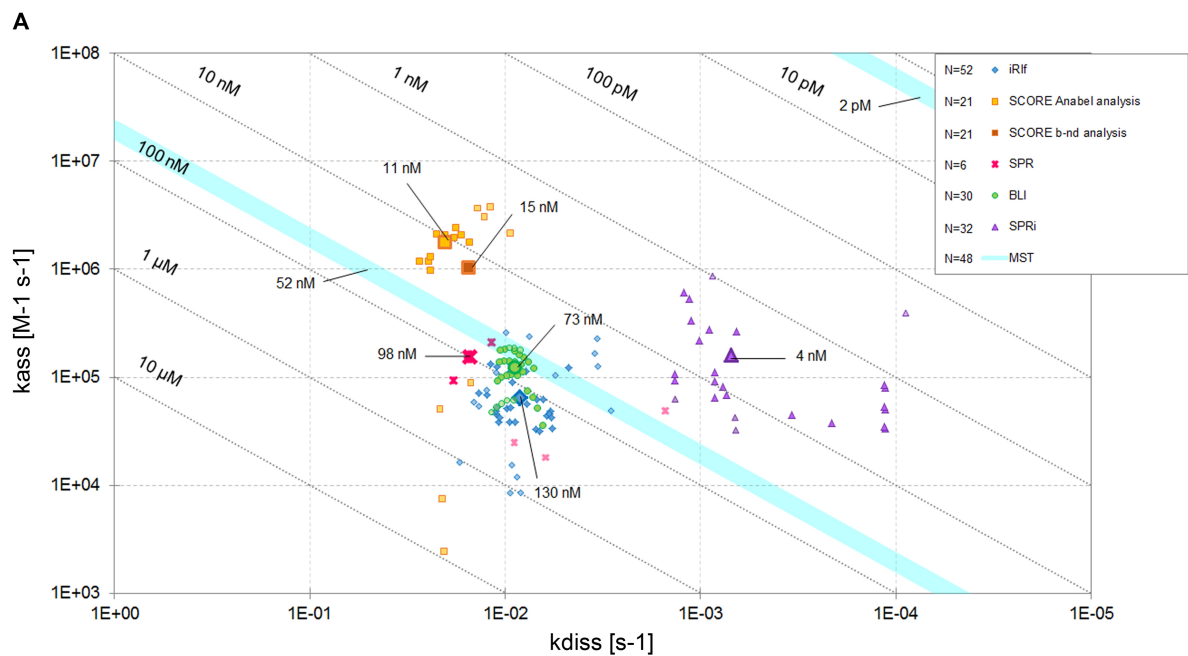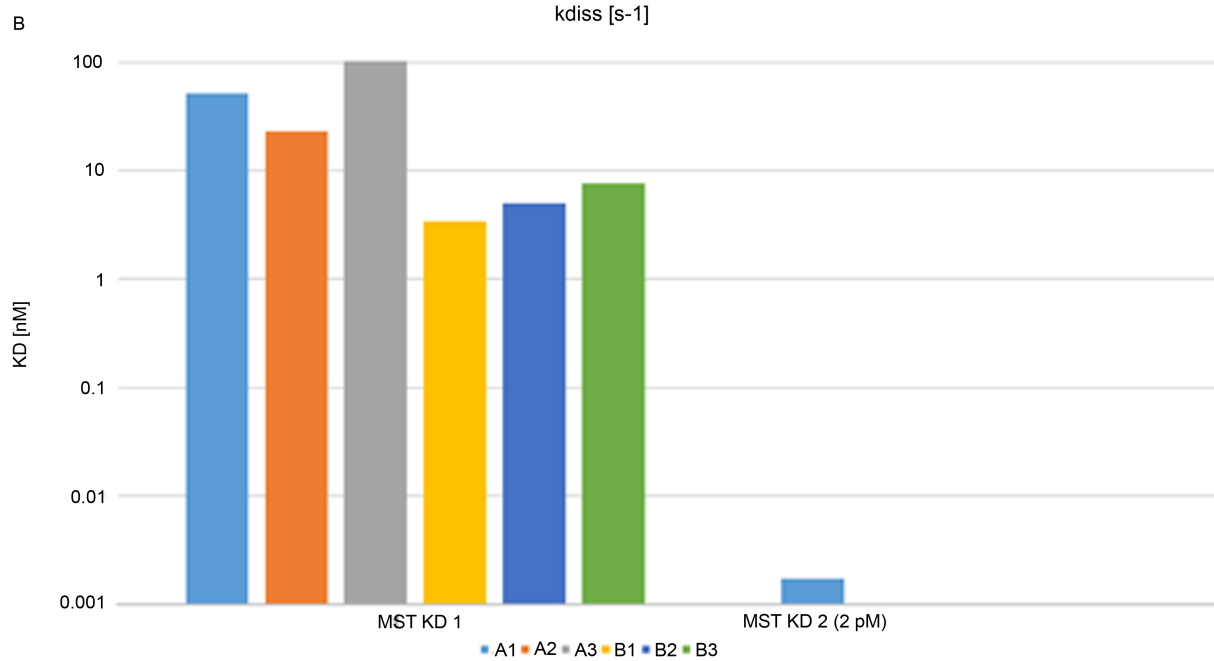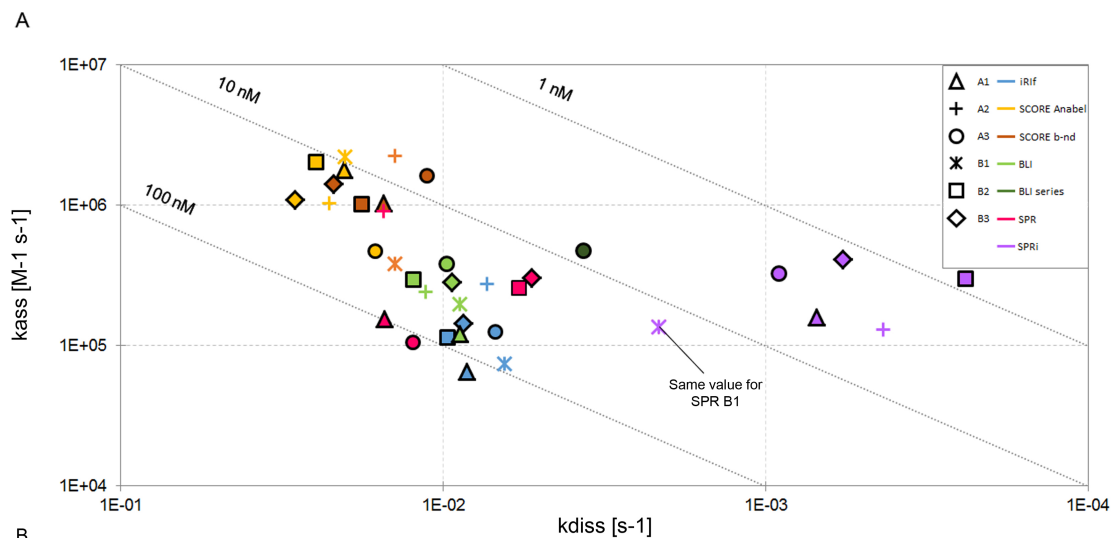
A
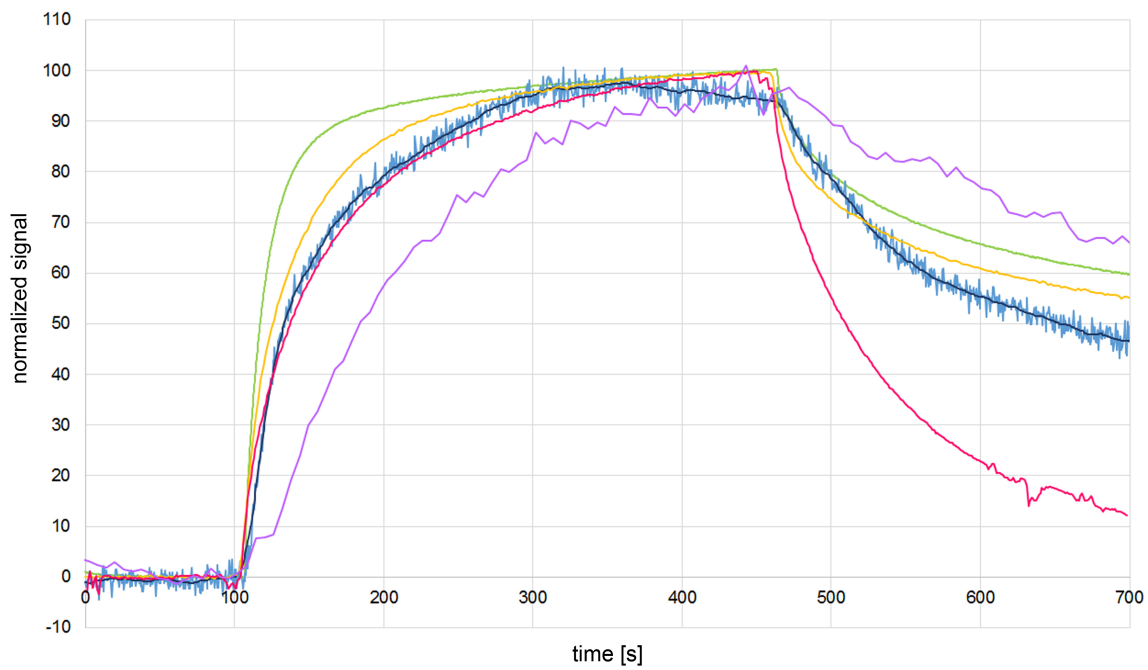
optical layer

biocompatible matrix

C6 aminomodified aptamer

biotinylated aptamer

streptavidin molecule

B

APTES/PDITC

high-refractive layer

glass substrate

C

NHS groups
biocompatible matrix
glass substrate

D

EDC/NHS

dextran matrix

gold layer
glass substrate

E

streptavidin layer
gold layer
glass substrate

A

B

Comparison of different label-free imaging high-throughput biosensing systems for aptamer binding measurements using thrombin aptamers as an example

Highlights

- Comparison of
  - 3 label-free high-throughput imaging systems
  - 2 label-free low-throughput non-imaging systems and
  - 1 in solution reference system

  for the determination of kinetic constants using thrombin aptamers

- Comparison of the influence of the analysis software used
- Comparison of the user influence
- High influence on the results by the user and from the assay conditions
- Recommendation to use at least two different systems and to analyze the kinetics best without prior knowledge of the assay and binding partners